Macrocyclic Hamilton receptor-shuttling dynamics in [2]rotaxanes

Maxime Douarre, Vicente Martí-Centelles, Cybille Rossy, Arnaud Tron, Isabelle Pianet, Nathan D Mcclenaghan

Macrocyclic Hamilton receptor-shuttling dynamics in [2]rotaxanes

Maxime Douarre,[a‡] Vicente Martí-Centelles,[a‡] Cybille Rossy,[a] Arnaud Tron,[a] Isabelle Pianet,*[b] and Nathan D. McClenaghan*[a]

[a]*Institut des Sciences Moléculaires, CNRS (UMR 5255), University of Bordeaux, Talence, France;* [b]*Université Bordeaux Montaigne, IRAMAT (UMR 5060), Maison de l'Archéologie, Pessac, France*

‡ These authors contributed equally. Corresponding Author *E-mail: nathan.mcclenaghan@u-bordeaux.fr (N.McC.), isabelle.pianet@u-bordeaux-montaigne.fr (I.P.)

Electronic Supplementary Information (ESI) available: experimental procedures, characterization data of **1**, **2**, and **4** (^{1}H, ^{13}C, VT NMR) and molecular modeling structures of rotaxanes **1**, **7**, and **8**.

Macrocyclic Hamilton receptor-shuttling dynamics in [2]rotaxanes

Inherent movement of a macrocycle comprising a multi-site hydrogen bonding Hamilton-type receptor in a series of [2]rotaxanes was investigated by dynamic and VT NMR. In these rotaxanes the varying nature and number of hydrogen-bond motifs and stations on the molecular axles influenced ring dynamics. Triazole stations interact selectively by hydrogen bonding with the isophthalamide amide bonds present in the Hamilton macrocycle and fast shuttling (72 kHz at 25 °C) was observed in a two station variant.

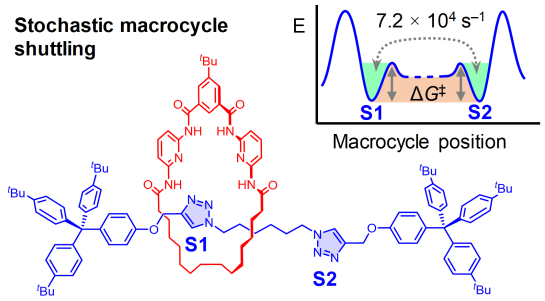

Keywords: molecular shuttle; rotaxane; hydrogen bonding; dynamic NMR; macrocycle

Introduction

Artificial molecular machines based on interlocked molecules have attracted much attention in the last decades, often such sophisticated structures mimic complex functions of biological systems. [1] In particular, [2]rotaxane systems comprising mobile macrocycles have been developed as molecular shuttles,[2–4] and determining shuttling parameters via dynamic NMR spectroscopy is an established approach.[5] This allowed determining the key role of ring movement in rotaxanes and obtaining detailed kinetic analyses providing key structure-property information in a number of different molecular machines,[5–8] including non-degenerate molecular shuttles used as switches in response to external stimulus,[2, 9, 10] and degenerate rotaxanes exhibiting spontaneous ring motion.[6, 11–17] Relevant works include Stoddart molecular shuttles

[5, 18–20], hydrogen-bonded molecular machines by Leigh,[3, 21, 22] Loeb's ring-through ring shuttling rotaxanes and related systems,[2, 23] Hirose's shuttling molecular machine studies on varing ring size and axle length,[6, 24], Coutrot's pioneering studies on shuttling effects in rotaxanes,[25] Brouwer's shuttling dynamics studies showing the complexity of that macrocycle shuttling events,[7] and Leigh's and Zerbetto's entropy-driven translational isomerism showing co-conformations in which the ring simultaneously interacts simultaneously with two stations.[26]

Among the different rotaxane formation methods, the Huisgen 1,3-dipolar cycloaddition involving reaction of alkyne and azide groups, also known as CuAAC "click" chemistry, has been extensively used as an efficient tool for the synthesis of interlocked molecules.[28, 29] In our previous studies, we employed this methodology to synthetize rotaxanes based on Hamilton-like macrocyclic receptor **3** on different axles (**8**) as well as Glaser coupling (**7**), however the ring shuttling dynamics in these systems were not explored.[30, 31] Herein, we enlarge the series to include double station rotaxane **1** and we focused on studying the stochastic molecular shuttling on the ensemble of the different axles via dynamic NMR spectroscopy to evaluate the effect of the different levels of ring–axle supramolecular interactions for rotaxanes **1**, **7** and **8** whose structures are shown in Figure 1. A schematic and qualitative potential energy surface representation of the macrocycle shuttling between two different energy stations is shown in Figure 1. The shuttling energy barrier depends only on the macrocycle binding affinity to the initial station and it is independent of the affinity to the arrival station,[12] therefore the shuttling rate is slower if the macrocycle–station binding affinity to the initial station is higher.[30, 31]

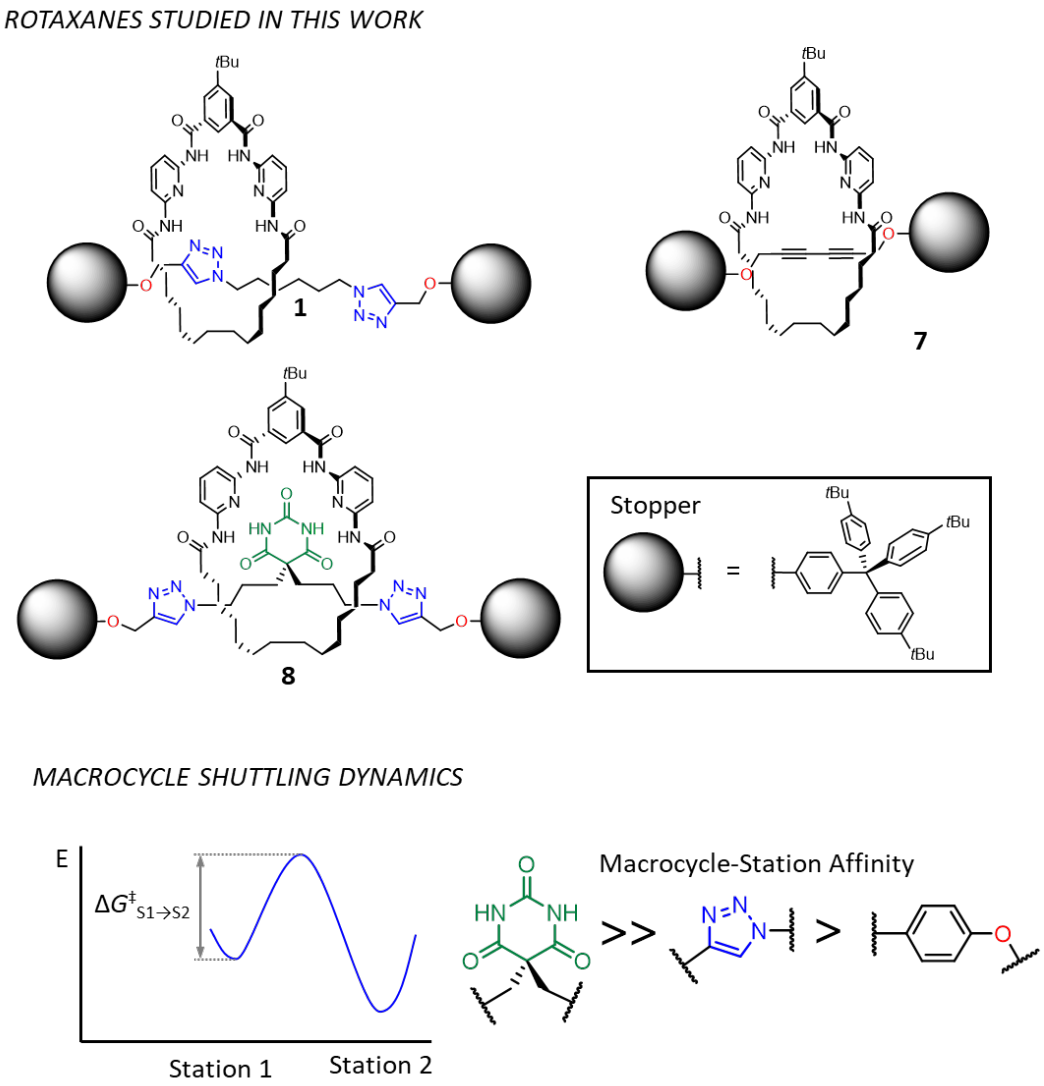

Figure 1. Top) Rotaxanes under investigation: **1** (synthesis developed in this work) and **7, 8** (synthesis previously reported).[30, 31] Bottom) Qualitative potential energy surface as a function of ring position (not to scale) showing the relative energy of the different stations and the $\Delta G^{\ddagger}_{S1\rightarrow S2}$ shuttling energy barrier. Energetics on non-bonding portions and possible alternative co-conformations involving the interaction with more than one station at the same time are not considered.

Results and discussion

The affinity of the macrocycle with the different stations is qualitatively represented in an idealized way in Figure 2. The macrocycle integrating a Hamilton receptor has a high

affinity towards the barbiturate station, as evidenced by binding studies with 5,5-diethylbarbiturate, where an interaction energy of –6.0 kcal/mol (K_{ass} = 23500 M^{-1} in $CHCl_3$) was determined.[31] In addition, the triazole ring can act as a hydrogen-bond acceptor station,[32, 33] and also the phenol-ether may act as an station with very weak affinity as the interaction of an amide with a phenol in $CHCl_3$ is a less favourable interaction ($\Delta\Delta G_{H\text{-}bond}$ = +3.6 kJ/mol).[34] Macrocycle shuttling in rotaxanes **1**, **7**, and **8** was investigated by VT NMR to study the effect of macrocycle–axle hydrogen bonding interaction strength of the different stations.

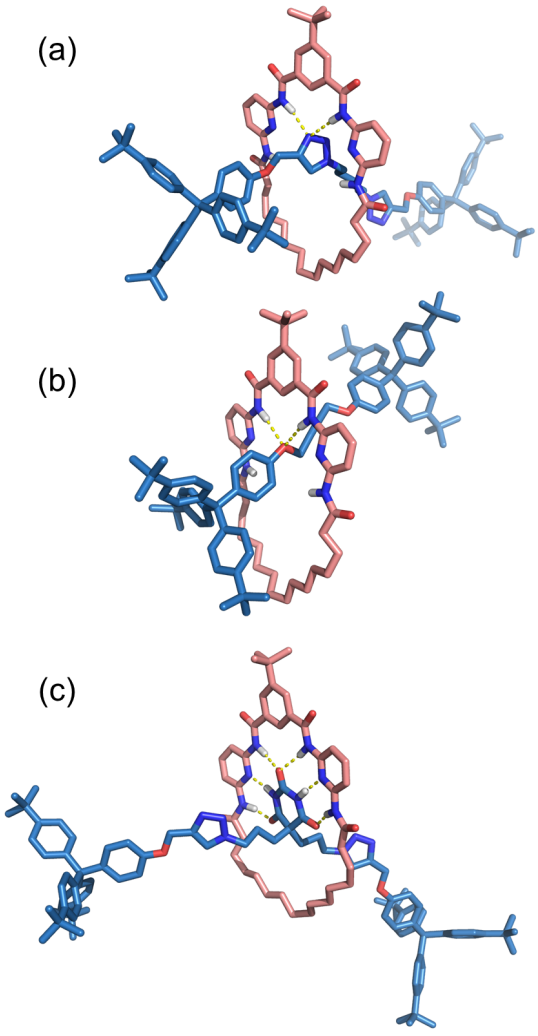

Figure 2. Representative molecular models of rotaxanes **1**, **7**, **8** showing the theoretical number of hydrogen bonds between axle and macrocycle. (a) **1**, (b) **7**, (c) **8**. Note:

Flexibility of both macrocyclic and axle components can result in alternative co-conformations (not shown) in this complex system.

Rotaxane **1** comprises the Hamilton-like macrocyclic receptor **3** [31] and a symmetrical axle integrating two triazole groups (Scheme 1). Initial attempts to prepare rotaxane **1** from 1,6-diazidehexane **6** and stopper **5** involving two-click reactions in the presence of macrocycle **3** and Cu(I) yield a complex mixture and no evidence of formation of [2]rotaxane **1** (or the corresponding [3]rotaxane) presumably associated to the low rotaxane formation yield and large formation of by-products (see Scheme 1). To facilitate the formation of the rotaxane with fewer possible side reactions, a different synthetic strategy was adopted. Synthesis involved a CuAAC "click" active template rotaxane formation involving alkyne stopper **5** and azide-terminated half-axle **4** in an excellent 86% yield, prepared from commercial 1,6-dibromohexane.[35] Using this approach one triazole moiety is already present in the azide half-axle **4** and the second triazole ring is created in the rotaxane formation step.

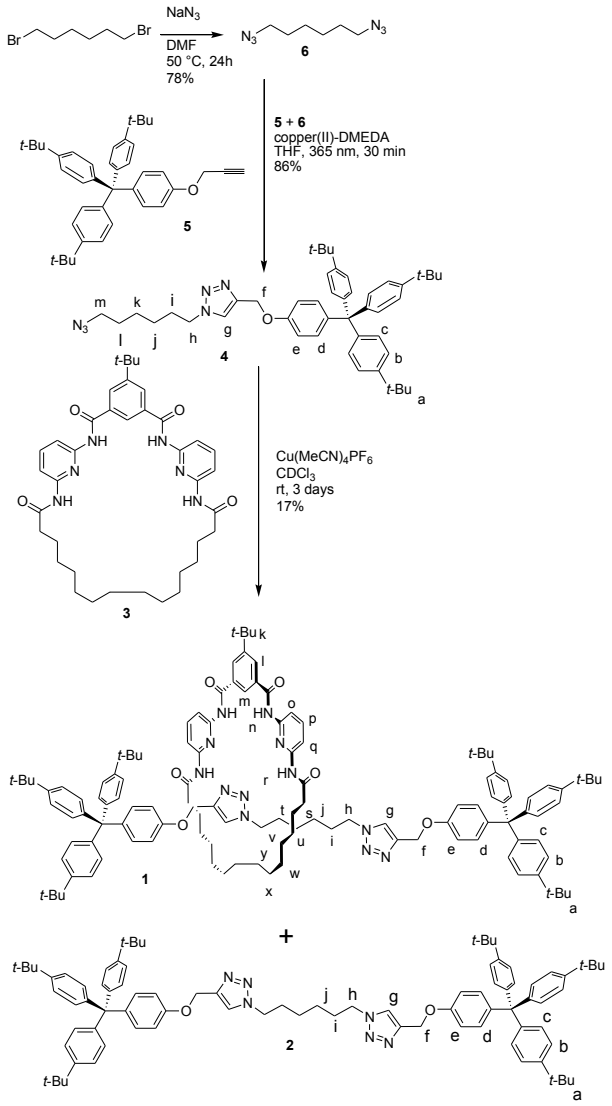

Scheme 1. Synthesis of rotaxane **1** and free axle **2** side-product via a click reaction. Letters in structures refer to ^{1}H NMR attributions. DMEDA = *N*,*N*'-dimethylethylendiamine.

Complexation of copper(I) by macrocycle **3** allows CuAAC "click" active template rotaxane formation.[30] Rotaxane **1** and the axle side-product (**3**) were isolated by column chromatography (SiO_2: CH_2Cl_2/ethyl acetate 10:0 to 8:2, v/v) in 17% and 58% yields, respectively. The obtained moderate yield for rotaxane formation was comparable to the obtained 20% yield for the homologue **7**, also involving a CuAAC

"click" active template rotaxane formation reaction.[30] We note in passing that, undoubtedly due to the relatively large macrocycle size and monodentate pyridine chelator, the obtained yield for these systems is low compared to certain other complex interlocked structures that have >90% rotaxane formation yield, for example based on small macrocycles and strong bipyridine chelators.[29, 36]

Rotaxane **1** was fully characterized by 1D- and 2D-NMR, and mass spectrometry (see electronic supporting information, ESI). The ^{1}H NMR spectrum of rotaxane **1** (Figure 3) shows downfield shifts of isophthalamide NH ($\Delta\delta$ = 1.08 ppm, *n*) and CH ($\Delta\delta$ = 0.84 ppm, *m*) signals with respect to non-interlocked macrocycle **3**. This confirms the existence of a selective hydrogen-bonding interaction between the triazole nitrogen atom in axle **2** and the isophthalamide motif in macrocycle **3** (Figure 3). In contrast, the amide NH *r* signal shows an upfield shift of $\Delta\delta$ = –0.18 ppm, suggesting that instead of participating in a hydrogen bonding interaction the proton is shielded by the triazole ring, as observed in the molecular model of rotaxane **1** (see Figure S19). The cartoon representation in Figure 3 shows a possible co-conformation as flexibility of both macrocyclic and axle components can result in alternative conformations resulting in a complex system.

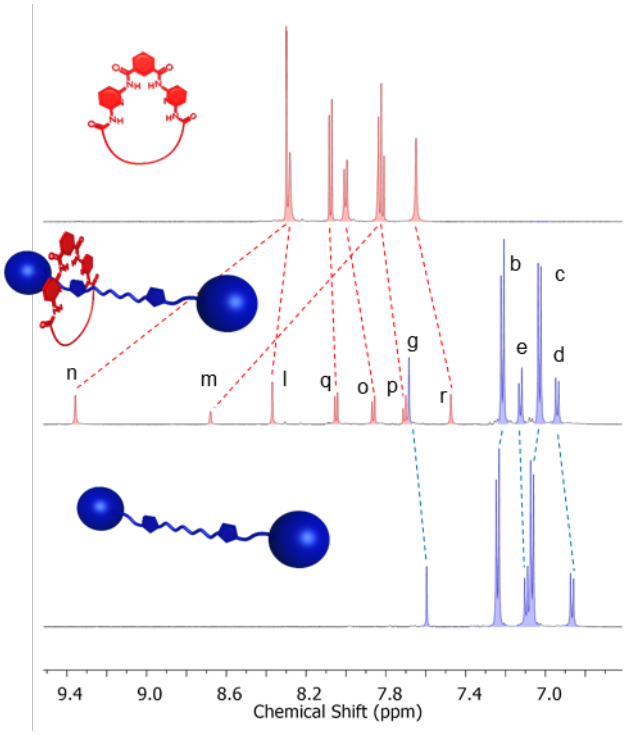

Figure 3. Partial ^{1}H NMR (600 MHz, TCE-d_2, rt) spectra of axle **2** (bottom), rotaxane **1** (middle) and macrocycle **3** (top). Designation of the signals is described in Scheme 1.

Additionally, DOSY NMR were performed in TCE-d_2 at 25 °C. Proton resonances corresponding to the constituent components in rotaxane **1** have the same diffusion coefficient of (1.14×10^{-6} cm^2/s, hydrodynamic radius = 10.4 Å), which is consistent with the interlocked nature of rotaxane **1** (see Figures S9-S12) and smaller compared to free macrocycle **3** (1.82×10^{-6} cm^2/s, hydrodynamic radius = 6.5 Å) and axle **2** (1.20×10^{-6} cm^2/s, hydrodynamic radius = 9.9 Å).

On cooling a solution of rotaxane **1** in CD_2Cl_2 from 25 °C to –40 °C (600 MHz spectrometer), only one set of signals was observed indicating fast exchange of the different co-conformation of the macrocycle and axle. A careful analysis of the shapes of the signals shows broadening of resonances, especially the methylene groups *f* and *h* next to the triazole moieties, suggesting rapid macrocycle shuttling between the two

triazole groups that would act as stations. We repeated the same experiment in more viscous TCE-d_2 (1.84 cP for TCE-d_2 and 0.43 cP for CD_2Cl_2)[37] and a lower dielectric constant (8.20 for TCE-d_2 and 8.9 for CD_2Cl_2).[37] Cooling down to – 30 °C also results in one set of signals with enhanced signal broadening. The methylene group *f*, that is close to the triazole proton showed the most significant broadening (Table 1).

Table 1. Peak width at half height for protons *f* and *a* at different temperatures of rotaxane **1** in CD_2Cl_2 and TCE-d_2.

	CD_2Cl_2		TCE-d_2	
T (°C)	*f* $\nu_{1/2}$ (Hz)	*a* $\nu_{1/2}$ (Hz)	*f* $\nu_{1/2}$ (Hz)	*a* $\nu_{1/2}$ (Hz)
25	1.73	0.99	3.23	1.48
10	2.90	2.02	5.39	2.84
0	2.44	1.30	6.56	2.57
–10	3.06	1.31	9.29	3.14
–20	4.00	1.53	19.67	4.49
–30	5.34	1.97	31.65	8.33
–40	10.50	2.51	—	—

As fast exchange slows down on cooling, a significant broadening of signals is observed but the coalescence temperature is not reached. (Note: Technical limitations preclude further lowering the temperature). However, the observed broadening of signals in TCE-d_2 is adequate for determining the shuttling exchange rate constant. In this case, $k > \upsilon_{S1\text{-}S2}$ and the process is slow enough to contribute to its width. The exchange rate constant *k* can be obtained using Equation 1.[38]

$$k \approx \frac{\pi \upsilon_{\upsilon S1-S2}{}^2}{2(\Delta\upsilon - \Delta\upsilon_{ref})} \quad (1)$$

In Equation 1, $\Delta\upsilon$ is the peak width at half-height, $\Delta\upsilon_{ref}$ is the peak width at half height of a non-exchanging reference. The *t*-Bu signal peak *a* was chosen as the non-exchanging. $\upsilon_{S1\text{-}S2}$ is the peak separation of *f* and *f*' after coalescence and can be

estimated as $\upsilon_{S1\text{-}S2}$ =2×(υ_{rotax} – υ_{axle}) = 232 Hz (0.386 ppm in the 600 MHz spectrometer) considering that the observed chemical shift in the rotaxane (5.348 ppm, υ_{rotax}) is the average of "free" and "occupied" stations and the chemical shift of the free station has been estimated from the free axle observed chemical shift (5.16 ppm, υ_{axle}). Signals were fitted to Lorentzian peaks to obtain the width at half height and the corresponding exchange rate constants *k* obtained using equation 1 (Figure 4a). Thermodynamics of the macrocycle shuttling process can be obtained from the *k* values at different temperatures by an Eyring plot (Figure 4b). From this plot, a value of $\Delta H^{\ddagger}$ = 7.4 kcal/mol and $\Delta S^{\ddagger}$ = –11.5 cal/mol K are obtained. These parameters allow extrapolating at 25 °C a value of $\Delta G^{\ddagger}_{25\,^{\circ}C}$ = 10.8 kcal/mol that corresponds to an exchange rate constant *k* = 72000 s^{-1}. Note that the interaction between amide (ring)-triazole (axle) has not been observed in related systems.[27] Probably the enhanced donor ability of macrocycle **3** could be the reason of the observed ring-thread affinity between the amide and the triazole.

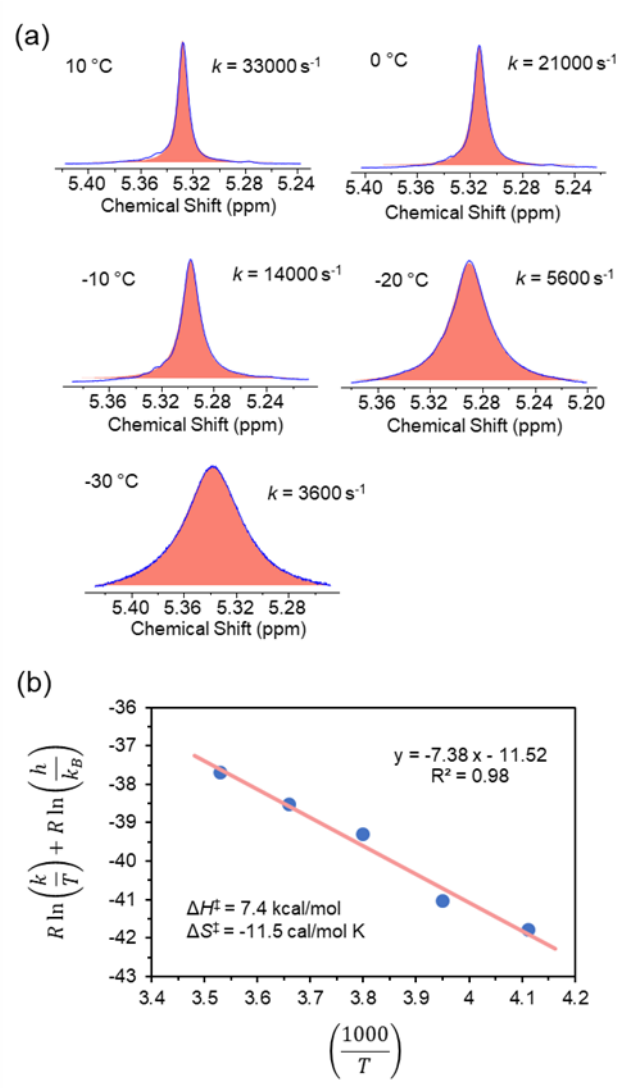

Figure 4. Determination of shuttling rate parameters for rotaxane **1** (a) Fittings to Lorentzian peaks of ^{1}H NMR signal *f* at different temperatures (600 MHz, TCE-d_2) and the corresponding exchange rate constants *k*. Fittings displayed as a dashed area and experimental data in a solid line. (b) Eyring plot of the exchange rate constants *k*.

Efforts to obtain precise shuttling rate constants or macrocycle rocking rate constants by VT NMR spectroscopy for rotaxanes **7** and **8** in different solvents ($CDCl_3$, CD_2Cl_2, TCE-d_2, DMSO-d_6, etc.) were unsuccessful as coalescence was not reached. As such, only qualitative shuttling information could be obtained for rotaxanes **7** and **8**. Weaker interaction of the isophthalamide with the phenol-ether stations in rotaxane **7** results in

insignificant signal broadening on cooling **7** in CD_2Cl_2 (Figure S16), consistent with very fast macrocycle shuttling, which is anticipated to be faster than in **1**. In the case of rotaxane **8**, a stronger interaction was observed between the barbiturate station and the Hamilton receptor motif. Indeed, even in a competitive solvent mixture ($CDCl_3$/MeOD/D_2O 45:45:10 v/v, Figure S17) or heating in a very strongly hydrogen bonding solvent (DMSO-d_6, Figure S18), which should weaken hydrogen bonding interactions between the two interlocked components, the macrocycle remains predominantly positioned at the barbiturate station. No specific evidence points to even a minor population on the triazole stations.[20] The corresponding thermodynamic equilibrium constant between the barbiturate station the triazole stations would be largely biased towards the barbiturate station. As the shuttling energy barrier only depends on the starting station and not the end station,[5] the shuttling rate from the triazole stations to the barbiturate station is predicted to be equivalent to that determined for rotaxane **1** with occasionally shuttling from the barbiturate station the triazole stations. This rate would be much slower and estimated by molecular modeling to be in the one shuttling event per second timescale (see Figure S19 in the Supporting Information). The different numerous examples of rotaxane structures reported in the literature fall approximate in the range of 8 kcal/mol to 20 kcal/mol, resulting in shuttling rates from $<1\ s^{-1}$ to $>10^6\ s^{-1}$.[1] For hydrogen bonding rotaxanes, they typically have an activation energy limited by bond breaking between macrocycle and initial station typically in the range 11–12 kcal/mol for weakly binding stations,[3, 12, 17, 39–41] and higher (16.2 kcal/mol) for the high affinity fumaramide station,[12] although this barrier can be lower for specific fumaramide station rotaxanes (13.4 kcal/mol).[14]

Conclusions

In summary, herein we report the study of macrocycle shuttling in rotaxanes featuring the Hamilton-type hydrogen-bonding receptor (**1**, **7**, and **8**). The rotaxanes have different hydrogen bonding affinities between the axle stations and the macrocycle isophthalamide motifs. These different affinities result in dramatic changes in the macrocycle shuttling rates at 25 °C from the different stations in the following order: barbiturate (**9**) < triazole (**1**) < phenol (**8**). Information on macrocycle-axle interactions and resulting ring dynamics could prove useful in introducing predetermined macrocycle shuttling rates in 2-station rotaxanes.

Experimental

Materials and methods

All chemicals and solvents were obtained from commercial sources and used without further purification unless a specific procedure is described. Dry solvents were obtained using solvent purification system inert® PureSolv Model PS-MD-5. Mass spectra and NMR were performed in the CESAMO analytical facilities (Bordeaux, France).

NMR

^{1}H and ^{13}C NMR spectra were recorded on a Bruker Avance I 300 MHz (300 MHz ^{1}H, 75 MHz ^{13}C), Bruker Avance II 400 MHz (400 MHz ^{1}H, 100 MHz ^{13}C); or Bruker Avance III 600 MHz (600 MHz ^{1}H, 150 MHz ^{13}C) spectrometer. Chemical shifts are reported in ppm and referenced to the solvent residual peaks. For the assignment of signals, the following abbreviations are used are s = singlet, d = doublet and t = triplet. DOSY NMR was performed in a Bruker Avance III 600 spectrometer using the

standard Bruker TopSpin 2D Stimulated Echo experiment using bipolar gradients (stebpgp1s) for diffusion measurements at 25 °C. The diffusion parameters were optimized to obtain a >70% on signal-intensity decay. From the DOSY diffusion coefficient, the hydrodynamic radius was obtained by using the Stokes–Einstein equation R = kT/(6πηD). VT NMR was performed in a Bruker Avance III 600 spectrometer, technical limitations preclude lowering the temperature below –40 °C.

Mass spectrometry

Electrospray spectra (ESI) were recorded on a Qexactive (Thermo) mass spectrometer. The instrument is equipped with an ESI source and spectra were recorded in positive mode. The spray voltage was maintained at 3200 V and capillary temperature set to 320 °C. Samples were introduced by injection through a 20 μL loop into a 300 μL/min flow of methanol from the LC pump.

VT NMR and exchange rate constant calculation

The $\Delta G^{\ddagger}$ at 25 °C was obtained to all systems by interpolation/extrapolation using Eyring plot using from the measured exchange rate constants (equations 2 and 3).[42]

$$R \ln\left(\frac{k_{ex}}{T}\right) + R\, ln\left(\frac{h}{k_{\mathrm{B}}}\right) = -\Delta H^{\ddagger}\left(\frac{1}{T}\right) + \Delta S^{\ddagger} \qquad (2)$$

With R = 1.99 cal mol^{-1} K^{-1}, $h = 6.63 \times 10^{-34}$ J s and $k_{\mathrm{B}} = 1.23 \times 10^{-23}$ J K^{-1} and a factor of 1000 in the enthalpic term to use the kcal.mol^{-1}units in $\Delta H^{\ddagger}$, equation 2 converts to equation 3.

$$1.99 \ln\left(\frac{k_{ex}}{T}\right) - 47.18 \frac{\mathrm{cal}}{\mathrm{mol\,K}} = -\Delta H^{\ddagger}\left(\frac{1000}{T}\right) + \Delta S^{\ddagger} \qquad (3)$$

The exchange rate constant k can be obtained using equation 1.[38] An approximate

value for $\upsilon_{S1\text{-}S2}$ has been obtained assuming that in the rotaxane the observed chemical shift is the average of "free" and "occupied" station and the chemical shift of the free station has been estimated from the free axle.

Molecular Modelling

Structures were minimized with the MMFF force field using the Spartan '18 software.[43] The isophthalamide motif in the macrocycle was constrained to be planar. The molecular models allowed determining the number of hydrogen bonds between the macrocycle and thread for the different rotaxanes described in this research (see ESI).

Synthetic procedures

1,6-Diazidehexane **6**, alkyne stopper **5**, Hamilton-like macrocyclic receptor **3** and rotaxanes **7**, **8** and **9** were prepared using literature procedures.[30, 31, 44, 45]

*Synthesis of rotaxane **1** and axle **2***

Macrocycle **3** (43 mg, 0.0657 mmol, 1.1 eq.) and $Cu(MeCN)_4PF_6$ (25 mg, 0.0671 mmol, 1.1 eq.) are dissolved in anhydrous chloroform (4 mL) previously degassed with gentle N_2 bubbling for 15 min. Solid azide **4** (43 mg, 0.0605 mmol, 1 eq.) and alkyne **5** (47.5 mg, 0.0875, 1.4 eq.) were simultaneously added to the mixture in one portion. The reaction mixture was stirred at room temperature for 3 days in the dark under N_2 atmosphere. The reaction mixture was quenched with 1 mL of a solution of EDTA (1M) in concentrated ammonium hydroxide (35%) and stirred at room temperature for 30 min. The mixture was diluted with dichloromethane (40 mL) and the organic layer was washed successively with water (2 × 50 mL) and brine (1 × 50 mL). The organic layer was dried over magnesium sulfate, filtered and concentrated *in vacuo*. Purification by silica gel column chromatography (DCM/EtOAc, 10:0 to 8:2, v/v) afforded double-

station rotaxane **1** as a colorless solid (13 mg, 17% yield) and axle **2** as a colorless solid (44 mg, 58% yield).

Rotaxane **1:** **^{1}H NMR** (600 MHz, CD_2Cl_2) δ 9.34 (s, 2H, H_n), 8.60 (brs, 1H, H_m), 8.34 (d, J = 1.4 Hz, 2H, H_l), 8.02 (d, J = 8.0 Hz, 2H, H_q), 7.84 (d, J = 8.0 Hz, 2H, H_o), 7.69 (s, 2H, H_g), 7.67 (t, J = 8.0 Hz, 2H, H_p), 7.56 (brs, 2H, H_r), 7.23 (d, J = 8.5 Hz, 12H, H_b), 7.16 (d, J = 8.9 Hz, 4H, H_e), 7.10 (d, J = 8.5 Hz, 12H, H_c), 6.93 (d,J = 8.9 Hz, 4H, H_d), 5.32 (bs 4H, H_f), 4.17 (t, J = 7.1 Hz, 4H, H_h), 2.11 (t, J = 7.8 Hz, 4H, H_s), 1.60 (m, 8H, H_t + H_i), 1.41 (s, 9H, H_k), 1.28 (s, 54H, H_a), 1.27 – 1.23 (m, 20H, $H_{u\text{-}y}$), 1,08 (m, 4H, H_j). **^{13}C NMR** (151 MHz, CD_2Cl_2) δ 171.9, 165.5, 156.6, 153.8, 150.8, 150.3, 149.0, 145.0, 144.8, 141.5, 141.0, 134.6, 132.7, 130.9, 130.5, 124.9, 123.4, 122.0, 114.2, 110.2, 109.7, 63.7, 63.1, 50.8, 38.0, 35.7, 34.8, 31.7, 31.5, 30.3, 29.3, 29.2, 29.1, 29.0, 28.7, 26.1, 25.5. **HRMS** (ESI): calcd for $C_{124}H_{154}N_{12}O_6$+H^+ $[M+H]^+$ m/z = 1908.2187, found m/z = 1908.2166.

Axle **2**: **^{1}H NMR** (600 MHz, TCE-d_2) δ 7.60 (s, 2H, H_g), 7.25 (d, J = 8.6 Hz, 12H, H_b), 7.10 (d, J = 8.9 Hz, 4H, H_d), 7.07 (d, J = 8.6 Hz, H_c), 6.87 (d, J = 9.0 Hz, 4H, H_e), 5.16 (s, 4H, H_f), 4.32 (t, J = 7.1 Hz, 4H, H_h), 1.89 (m, 4H, H_i), 1.38 – 1.33 (m, 4H, H_j), 1.31 (s, 54H, H_a). **^{13}C NMR** (75 MHz, $CDCl_3$) δ 156.3, 148.5, 144.6, 144.2, 140.3, 132.5, 130.8, 124.2, 122.6, 113.4, 63.20, 62.18, 50.2, 34.4, 31.5, 30.1, 26.0. **HRMS (ESI)** calcd for $C_{86}H_{104}N_6O_2$+H^+ $[M+H]^+$ m/z = 1253.8294, found m/z = 1253.8278.

*Synthesis of azide **4***

Azide **4** was synthesized using a general copper-click procedure from Beniazza *et al.*[35] In a Schlenk tube, copper(II)-DMEDA complex (6.2 mg, 8.56 μmol, 1 mol%), alkyne **5** (465 mg, 0.856 mmol, 1 eq.) and azide **6** (1.44 g, 8.56 mmol, 10 eq.) were dissolved in THF (5 mL). The reaction mixture, protected from light by aluminium foil,

was then degassed by gentle argon bubbling for 20 minutes. The reaction mixture was irradiated at 365 nm using a TLC lamp placed at ~ 1 cm from the tube and stirred for 30 min at room temperature. The reaction mixture was diluted with EtOAc (50 mL) and washed successively with water (2 × 50 mL) and brine (1 × 50 mL). The organic layer was dried over magnesium sulfate, filtered and concentrated *in vacuo*. Purification by silica gel column chromatography (cyclohexane/EtOAc 10:0 to 9:1, v/v) afforded azide **4** as a colorless solid (526 mg, 86% yield). **^{1}H NMR** (300 MHz, $CDCl_3$) δ 7.59 (m, 1H, H_g), 7.23 (m, 6H, H_b), 7.09 (m, 8H, H_c + H_d), 6.86 (m, 2H, H_e), 5.19 (s, 2H, H_f), 4.37 (t, J = 7.2 Hz, 2H, H_h), 3.26 (t, J = 6.7 Hz, 2H, H_m), 1.94 (p, J = 7.3 Hz, 1H, H_i), 1.65 – 1.53 (m, 2H, H_l), 1.49 – 1.35 (m, 4H, H_k + H_j), 1.30 (s, 27H, H_a). **^{13}C NMR** (100 MHz, $CDCl_3$) 156.2, 148.5, 144.5, 144.2, 140.3, 132.5, 130.8, 124.2, 122.6, 113.4, 63.2, 62.2, 51.3, 50.4, 34.4, 31.5, 30.2, 28.7, 26.2, 26.2. **HRMS (ESI)** calcd for $C_{46}H_{58}N_6O+H^+$ $[M+H]^+$ m/z = 711.4745, found m/z = 711.4731.

Conflicts of interest

There are no conflicts to declare.

Acknowledgements

We thank the analytical facilities CESAMO (NMR and HRMS) of the Institut des Sciences Moléculaires, University of Bordeaux. This project has received funding from the European Union's Horizon 2020 research and innovation programme under the Marie Skłodowska-Curie grant agreement No. 796612. Equally, financial support from the Agence Nationale de la Recherche (project ANR-16-CE29-0011) and CNRS is gratefully acknowledged.

The Version of Record of this manuscript has been published and is available in SUPRAMOLECULAR CHEMISTRY, 2020, (Accepted 04 Oct 2020, Published online: 20 Oct 2020)

http://tandfonline.com/10.1080/10610278.2020.1834560

Notes and references

[1] Bruns, C. J.; Stoddart, J. F. The Stereochemistry of the Mechanical Bond. In *The Nature of the Mechanical Bond*; John Wiley & Sons, Inc.: Hoboken, NJ, USA, 2016; pp 471–554. https://doi.org/10.1002/9781119044123.ch5.

[2] Zhu, K.; O'Keefe, C. A.; Vukotic, V. N.; Schurko, R. W.; Loeb, S. J. A Molecular Shuttle That Operates inside a Metal-Organic Framework. *Nat. Chem.*, **2015**, *7* (6), 514–519. https://doi.org/10.1038/nchem.2258.

[3] Brouwer, A. M.; Frochot, C.; Gatti, F. G.; Leigh, D. A.; Mottier, L.; Paolucci, F.; Roffia, S.; Wurpel, G. W. H. Photoinduction of Fast, Reversible Translational Motion in a Hydrogen-Bonded Molecular Shuttle. *Science*, **2001**, *291* (5511), 2124–2128. https://doi.org/10.1126/science.1057886.

[4] Serreli, V.; Lee, C. F.; Kay, E. R.; Leigh, D. A. A Molecular Information Ratchet. *Nature*, **2007**, *445* (7127), 523–527. https://doi.org/10.1038/nature05452.

[5] Bruns, C. J.; Stoddart, J. F. *The Nature of the Mechanical Bond: From Molecules to Machines*; John Wiley & Sons: Hoboken, NJ, USA, 2016. https://doi.org/10.1002/9781119044123.

[6] Young, P. G.; Hirose, K.; Tobe, Y. Axle Length Does Not Affect Switching Dynamics in Degenerate Molecular Shuttles with Rigid Spacers. *J. Am. Chem. Soc.*, **2014**, *136* (22), 7899–7906. https://doi.org/10.1021/ja412671k.

[7] Kumpulainen, T.; Panman, M. R.; Bakker, B. H.; Hilbers, M.; Woutersen, S.; Brouwer, A. M. Accelerating the Shuttling in Hydrogen-Bonded Rotaxanes: Active Role of the Axle and the End Station. *J. Am. Chem. Soc.*, **2019**, *141* (48), 19118–19129. https://doi.org/10.1021/jacs.9b10005.

[8] Corra, S.; De Vet, C.; Groppi, J.; La Rosa, M.; Silvi, S.; Baroncini, M.; Credi, A. Chemical On/Off Switching of Mechanically Planar Chirality and Chiral Anion Recognition in a [2]Rotaxane Molecular Shuttle. *J. Am. Chem. Soc.*, **2019**, *141* (23), 9129–9133. https://doi.org/10.1021/jacs.9b00941.

[9] Da Ros, T.; Guldi, D. M.; Morales, A. F.; Leigh, D. A.; Prato, M.; Turco, R. Hydrogen Bond-Assembled Fullerene Molecular Shuttle. *Org. Lett.*, **2003**, *5* (5), 689–691. https://doi.org/10.1021/ol0274110.

[10] Keaveney, C. M.; Leigh, D. A. Shuttling through Anion Recognition. *Angew. Chem. Int. Ed.*, **2004**, *43* (10), 1222–1224. https://doi.org/10.1002/anie.200353248.

[11] Ghosh, A.; Paul, I.; Adlung, M.; Wickleder, C.; Schmittel, M. Oscillating Emission of [2]Rotaxane Driven by Chemical Fuel. *Org. Lett.*, **2018**, *20* (4), 1046–1049. https://doi.org/10.1021/acs.orglett.7b03996.

[12] Leigh, D. A.; Wong, J. K. Y.; Dehez, F.; Zerbetto, F. Unidirectional Rotation in a Mechanically Interlocked Molecular Rotor. *Nature*, **2003**, *424* (6945), 174–179. https://doi.org/10.1038/nature01758.

[13] Li, H.; Zhao, Y. L.; Fahrenbach, A. C.; Kim, S. Y.; Paxton, W. F.; Stoddart, J. F. Degenerate [2]Rotaxanes with Electrostatic Barriers. *Org. Biomol. Chem.*, **2011**, *9* (7), 2240–2250. https://doi.org/10.1039/c0ob00937g.

[14] Douarre, M.; Martí-Centelles, V.; Rossy, C.; Pianet, I.; McClenaghan, N. Regulation of Macrocycle Shuttling Rates in [2]Rotaxanes by Amino-Acid Speed Bumps in Organic-Aqueous Solvent Mixtures. *Eur. J. Org. Chem.*, **2020**, 5820–5827. https://doi.org/10.1002/ejoc.202000997.

[15] Paul, I.; Ghosh, A.; Bolte, M.; Schmittel, M. Remote Control of the Synthesis of a [2]Rotaxane and Its Shuttling via Metal□Ion Translocation. *ChemistryOpen*, **2019**, *8* (11), 1355–1360. https://doi.org/10.1002/open.201900293.

[16] Gholami, G.; Zhu, K.; Baggi, G.; Schott, E.; Zarate, X.; Loeb, S. J. Influence of Axle Length on the Rate and Mechanism of Shuttling in Rigid H-Shaped [2]Rotaxanes. *Chem. Sci.*, **2017**, *8* (11), 7718–7723. https://doi.org/10.1039/c7sc03736h.

[17] Berná, J.; Alajarín, M.; Marín-Rodríguez, C.; Franco-Pujante, C. Redox

Divergent Conversion of a [2]Rotaxane into Two Distinct Degenerate Partners with Different Shuttling Dynamics. *Chem. Sci.*, **2012**, *3* (7), 2314–2320. https://doi.org/10.1039/c2sc20488f.

[18] Coskun, A.; Friedman, D. C.; Li, H.; Patel, K.; Khatib, H. A.; Stoddart, J. F. A Light-Gated STOP-GO Molecular Shuttle. *J. Am. Chem. Soc.*, **2009**, *131* (7), 2493–2495. https://doi.org/10.1021/ja809225e.

[19] Jeppesen, J. O.; Perkins, J.; Becher, J.; Fraser Stoddart, J. Slow Shuttling in an Amphiphilic Bistable [2]Rotaxane Incorporating a Tetrathiafulvalene Unit. *Angew. Chem. Int. Ed.*, **2001**, *40* (7), 1216–1221. https://doi.org/10.1002/1521-3773(20010401)40:7<1216::AID-ANIE1216>3.0.CO;2-W.

[20] Stoddart, J. F. Mechanically Interlocked Molecules (MIMs)-Molecular Shuttles, Switches, and Machines (Nobel Lecture). *Angew. Chem. Int. Ed.*, **2017**, *56* (37), 11094–11125. https://doi.org/10.1002/anie.201703216.

[21] Panman, M. R.; Bakker, B. H.; Den Uyl, D.; Kay, E. R.; Leigh, D. A.; Buma, W. J.; Brouwer, A. M.; Geenevasen, J. A. J.; Woutersen, S. Water Lubricates Hydrogen-Bonded Molecular Machines. *Nat. Chem.*, **2013**, *5* (11), 929–934. https://doi.org/10.1038/nchem.1744.

[22] Hernández, J. V.; Kay, E. R.; Leigh, D. A. A Reversible Synthetic Rotary Molecular Motor. *Science*, **2004**, *306* (5701), 1532–1537. https://doi.org/10.1126/science.1103949.

[23] Zhu, K.; Baggi, G.; Loeb, S. J. Ring-through-Ring Molecular Shuttling in a Saturated [3]Rotaxane. *Nat. Chem.*, **2018**, *10* (6), 625–630. https://doi.org/10.1038/s41557-018-0040-9.

[24] Hirose, K.; Shiba, Y.; Ishibashi, K.; Doi, Y.; Tobe, Y. A Shuttling Molecular Machine with Reversible Brake Function. *Chem. Eur. J.*, **2008**, *14* (11), 3427–3433. https://doi.org/10.1002/chem.200702001.

[25] Busseron, E.; Romuald, C.; Coutrot, F. Bistable or Oscillating State Depending on Station and Temperature in Three-Station Glycorotaxane Molecular Machines. *Chem. Eur. J.*, **2010**, *16* (33), 10062–10073. https://doi.org/10.1002/chem.201000777.

[26] Bottari, G.; Dehez, F.; Leigh, D. A.; Nash, P. J.; Pérez, E. M.; Wong, J. K. Y.;

Zerbetto, F. Entropy-Driven Translational Isomerism: A Tristable Molecular Shuttle. *Angew. Chem. Int. Ed.*, **2003**, *42* (47), 5886–5889. https://doi.org/10.1002/anie.200352176.

[27] Evans, N. H.; Akien, G. R. Rapid and Simultaneous Synthesis of a Hydrogen Bond Templated [3]Rotaxane and Its Related [2]Rotaxane Molecular Shuttle. *Supramol. Chem.*, **2018**, *30* (2), 158–164. https://doi.org/10.1080/10610278.2017.1400031.

[28] Hänni, K. D.; Leigh, D. A. The Application of CuAAC "click" Chemistry to Catenane and Rotaxane Synthesis. *Chem. Soc. Rev.*, **2010**, *39* (4), 1240–1251. https://doi.org/10.1039/b901974j.

[29] Denis, M.; Goldup, S. M. The Active Template Approach to Interlocked Molecules. *Nat. Rev. Chem.*, **2017**, *1* (8), 1–17. https://doi.org/10.1038/s41570-017-0061.

[30] Tron, A.; Thornton, P. J.; Kauffmann, B.; Tucker, J. H. R.; McClenaghan, N. D. [2]Rotaxanes Comprising a Macrocylic Hamilton Receptor Obtained Using Active Template Synthesis: Synthesis and Guest Complexation. *Supramol. Chem.*, **2016**, *28* (9–10), 733–741. https://doi.org/10.1080/10610278.2015.1122194.

[31] Tron, A.; Thornton, P. J.; Rocher, M.; Jacquot De Rouville, H. P.; Desvergne, J. P.; Kauffmann, B.; Buffeteau, T.; Cavagnat, D.; Tucker, J. H. R.; McClenaghan, N. D. Formation of a Hydrogen-Bonded Barbiturate [2]-Rotaxane. *Org. Lett.*, **2014**, *16* (5), 1358–1361. https://doi.org/10.1021/ol500099u.

[32] Schulze, B.; Schubert, U. S. Beyond Click Chemistry-Supramolecular Interactions of 1,2,3-Triazoles. *Chem. Soc. Rev.*, **2014**, *43* (8), 2522–2571. https://doi.org/10.1039/c3cs60386e.

[33] Zheng, H.; Zhou, W.; Lv, J.; Yin, X.; Li, Y.; Liu, H.; Li, Y. A Dual-Response [2]Rotaxane Based on a 1,2,3-Triazole Ring as a Novel Recognition Station. *Chem. Eur. J.*, **2009**, *15* (47), 13253–13262. https://doi.org/10.1002/chem.200901841.

[34] Hunter, C. A. Quantifying Intermolecular Interactions: Guidelines for the Molecular Recognition Toolbox. *Angew. Chem. Int. Ed.*, **2004**, *43* (40), 5310–

5324. https://doi.org/10.1002/anie.200301739.

[35] Beniazza, R.; Lambert, R.; Harmand, L.; Molton, F.; Duboc, C.; Denisov, S.; Jonusauskas, G.; McClenaghan, N. D.; Lastécouères, D.; Vincent, J.-M. Sunlight-Driven Copper-Catalyst Activation Applied to Photolatent Click Chemistry. *Chem. Eur. J.*, **2014**, *20* (41), 13181–13187. https://doi.org/10.1002/chem.201404056.

[36] Lewis, J. E. M.; Beer, P. D.; Loeb, S. J.; Goldup, S. M. Metal Ions in the Synthesis of Interlocked Molecules and Materials. *Chemical Society Reviews*. Royal Society of Chemistry May 7, 2017, pp 2577–2591. https://doi.org/10.1039/c7cs00199a.

[37] Data from standard product datasheets.

[38] Gasparro, F. P. NMR Determination of the Rotational Barrier in N,N-Dimethylacetamide a Physical Chemistry Experiment. *J. Chem. Educ.*, **1977**, *54* (4), 258–261. https://doi.org/10.1021/ed054p258.

[39] Günbaş, D. D.; Brouwer, A. M. Degenerate Molecular Shuttles with Flexible and Rigid Spacers. *J. Org. Chem.*, **2012**, *77* (13), 5724–5735. https://doi.org/10.1021/jo300907r.

[40] Lane, A. S.; Leigh, D. A.; Murphy, A. Peptide-Based Molecular Shuttles. *J. Am. Chem. Soc.*, **1997**, *119* (45), 11092–11093. https://doi.org/10.1021/ja971224t.

[41] Berná, J.; Bottari, G.; Leigh, D. A.; Pérez, E. M. Amide-Based Molecular Shuttles (2001-2006). *Pure and Applied Chemistry*. International Union of Pure and Applied Chemistry January 2007, pp 39–54. https://doi.org/10.1351/pac200779010039.

[42] Williams, T. J.; Kershaw, A. D.; Li, V.; Wu, X. An Inversion Recovery NMR Kinetics Experiment. *J. Chem. Educ.*, **2011**, *88* (5), 665–669. https://doi.org/10.1021/ed1006822.

[43] Deppmeier, B.J.; Driessen, A.J.; Hehre, W. J.; Hehre, T. S.; Johnson, J. A.; Ohlinger, S.; Klunzinger, P. E. Spartan 18, build 1.3.0 (Feb 19 2019), Wavefunction Inc., 2019.

[44] Aucagne, V.; Hänni, K. D.; Leigh, D. A.; Lusby, P. J.; Walker, D. B. Catalytic "Click" Rotaxanes: A Substoichiometric Metal-Template Pathway to

Mechanically Interlocked Architectures. *J. Am. Chem. Soc.*, **2006**, *128* (7), 2186–2187. https://doi.org/10.1021/ja056903f.

[45] Díaz, D. D.; Rajagopal, K.; Strable, E.; Schneider, J.; Finn, M. G. "Click" Chemistry in a Supramolecular Environment: Stabilization of Organogels by Copper(I)-Catalyzed Azide-Alkyne [3 + 2] Cycloaddition. *J. Am. Chem. Soc.*, **2006**, *128* (18), 6056–6057. https://doi.org/10.1021/ja061251w.